
Bayesian Bits: Unifying Quantization and Pruning

Mart van Baalen^{*1} Christos Louizos^{*1} Markus Nagel¹ Rana Ali Amjad¹ Ying Wang¹ Tijmen Blankevoort¹
Max Welling¹

Abstract

We introduce Bayesian Bits, a practical method for joint mixed precision quantization and pruning through gradient based optimization. Bayesian Bits employs a novel decomposition of the quantization operation, which sequentially considers doubling the bit width. At each new bit width, the residual error between the full precision value and the previously rounded value is quantized. We then decide whether or not to add this quantized residual error for a higher effective bit width and lower quantization noise. By starting with a power-of-two bit width, this decomposition will always produce hardware-friendly configurations, and through an additional 0-bit option, serves as a unified view of pruning and quantization. Bayesian Bits then introduces learnable stochastic gates, which collectively control the bit width of the given tensor. As a result, we can obtain low bit solutions by performing approximate inference over the gates, with prior distributions that encourage most of them to be switched off. We further show that, under some assumptions, L_0 regularization of the network parameters corresponds to a specific instance of the aforementioned framework. We experimentally validate our proposed method on several benchmark datasets and show that we can learn pruned, mixed precision networks that provide a better trade-off between accuracy and efficiency than their static bit width equivalents.

1. Introduction

To reduce the computational cost of neural network inference, quantization and compression techniques are often applied before deploying a model in real life. The former

reduces the bit width of weight and activation tensors by quantizing floating-point values onto a regular grid, allowing the use of cheap integer arithmetic, while the latter aims to reduce the total number of multiply-accumulate (MAC) operations required by reducing the number of network parameters. We refer the reader to [Krishnamoorthi \(2018\)](#) and [Kuzmin et al. \(2019\)](#) for overviews of hardware-friendly quantization and compression techniques, respectively.

In quantization, the default assumption is that all layers should be quantized to the same bit width. While it has long been understood that low bit-width quantization can be achieved by keeping the first and last layers of a network in higher precision ([Shayer et al., 2017](#); [Choi et al., 2018](#)), recent work ([Dong et al., 2019b](#); [Uhlich et al., 2020](#); [Wang et al., 2019](#)) has shown that carefully selecting the bit width of each tensor can yield a better trade-off between accuracy and complexity. Since the choice of quantization bit width for one tensor affects the quantization sensitivity of all other tensors, the choice of bit width cannot be made without regarding the rest of the network.

The number of possible bit width configurations for a neural network is exponential in the number of layers in the network. Therefore, we cannot exhaustively search all possible configurations and pick the best one. Several approaches to learning the quantization bit widths from data have been proposed, either during training ([Uhlich et al., 2020](#); [Louizos et al., 2017](#)), or on pre-trained networks ([Wang et al., 2019](#); [Dong et al., 2019b;a](#)). However, these works do not consider the fact that commercially available hardware typically only supports efficient computation in power-of-two bit widths (see e.g., [Ignatov et al. \(2019\)](#) for a mobile hardware overview and [Moons et al. \(2017\)](#) for a method to perform four 4-bit multiplications in a 16-bit hardware multiplication unit.)

In this paper, we introduce a novel decomposition of the quantization operation. This decomposition exposes all hardware-friendly (i.e., power-of-two) bit widths individually by recursively quantizing the residual error of lower bit width quantization. The quantized residual error tensors are then added together into a quantized approximation of the original tensor. This allows for the introduction of learnable stochastic gates: by placing a gate on each of the quantized

^{*}Equal contribution ¹Qualcomm AI Research, an initiative of Qualcomm Technologies, Inc. and/or its subsidiaries. Correspondence to: Mart van Baalen <mart@qti.qualcomm.com>, Christos Louizos <clouizos@qti.qualcomm.com>, Tijmen Blankevoort <tijmen@qti.qualcomm.com>.

residual error tensors, the effective bit width can be controlled, thus allowing for data-dependent optimization of the bit width of each tensor. We then extend the gating formulation such that not only the residuals, but the overall result of the quantization is gated as well. This facilitates for “zero bit” quantization and serves as a unified view of pruning and quantization. We cast the optimization of said gates as a variational inference problem with prior distributions that favor quantizers with low bit widths. Lastly, we provide an intuitive and practical approximation to this objective, that is amenable to efficient gradient-based optimization. We experimentally validate our method on several models and datasets and show encouraging results, both for end-to-end fine-tuning tasks as well as post-training quantization.

2. Unifying quantization and pruning with Bayesian Bits

Consider having an input x in the range of $[\alpha, \beta]$ that is quantized with a uniform quantizer with an associated bit width b . Such a quantizer can be expressed as

$$x_q = s \lfloor x/s \rfloor, \quad s = \frac{\beta - \alpha}{2^b - 1} \quad (1)$$

where s is the step-size of the quantizer that depends on the given bit width b . How can we learn the number of bits b , while respecting the hardware constraint that b should be a power of two? One possible way would be via “decomposing” the quantization operation in a way that exposes all of the appropriate bit widths. In the following section, we will devise a simple and practical method that realizes such a procedure.

2.1. Mixed precision gating for quantization and pruning

Consider initially quantizing x with $b = 2$:

$$x_2 = s_2 \lfloor x/s_2 \rfloor, \quad s_2 = \frac{\beta - \alpha}{2^2 - 1}. \quad (2)$$

How can we then “move” to the next hardware friendly bit width, i.e. $b = 4$? We know that the quantization error of this operation will be $x - x_2$, and it will be in $[-s_2/2, s_2/2]$. We can then consider encoding this residual error according to a fixed point grid that has a length of s_2 and bins of size $s_2/(2^2 + 1)$

$$.pdfilon_4 = s_4 \lfloor (x - x_2)/s_4 \rfloor, \quad s_4 = \frac{s_2}{2^2 + 1}. \quad (3)$$

By then adding this quantized residual to x_2 , i.e. $x_4 = x_2 + .pdfilon_4$ we obtain a quantized tensor x_4 that has double the precision of the previous tensor, i.e. an effective bit width of $b = 4$ with a step-size of $s_4 = \frac{\beta - \alpha}{(2^2 - 1)(2^2 + 1)} = \frac{\beta - \alpha}{2^4 - 1}$. To understand why this is the case, we can proceed as

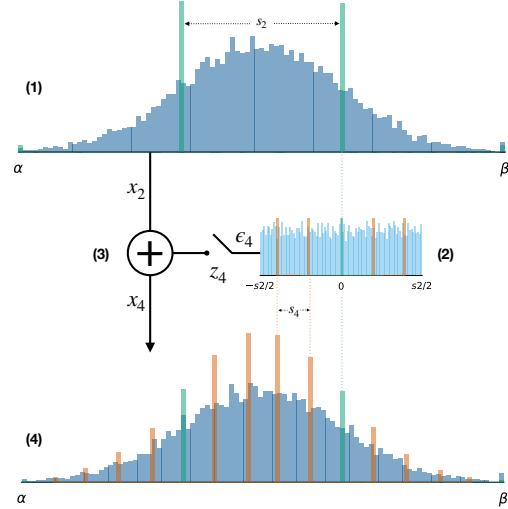


Figure 1. Illustration of our decomposition. The input floating point values x are clipped to the learned range $[\alpha, \beta]$ (dark blue histograms), and are quantized to 2 bits into x_2 (green histograms) (1). To accommodate the 2^2 grid points of the 2 bit quantization grid, the range is divided into $2^2 - 1$ equal parts, hence $s_2 = \frac{\beta - \alpha}{2^2 - 1}$. Next, the residual error $x - x_2$ is computed (light blue histogram), and quantized onto the 4 bit grid (2), resulting in the quantized residual error tensor $.pdfilon_4$. To accommodate the points of the 4 bit quantization grid, the range is divided into $2^4 - 1$ equal parts. Note that $(2^4 - 1) = (2^2 - 1)(2^2 + 1)$, thus we can compute s_4 as $s_2/(2^2 + 1)$. This can alternatively be seen as dividing the residual error, with range bounded by $[-s_2/2, s_2/2]$, into $2^2 + 1$ equal parts. Values in the quantized residual error equal to 0 correspond to points on the 2 bit grid, other values correspond to points on the 4 bit grid (orange histogram). Next, the quantized residual error is added to x_2 if the 4-bit gate z_4 is equal to 1 (3), resulting in the 4-bit quantized tensor x_4 (4). NB: quantization histograms and floating point histograms are not on the same scale.

follows: the output of $s_2 \lfloor x/s_2 \rfloor$ will be an integer multiple of s_4 , as $s_2 = s_4(2^2 + 1)$, thus it will be a part of the four bit quantization grid as well. Furthermore, the quantized residual is also an integer multiple of s_4 , as $\lfloor (x - x_2)/s_4 \rfloor$ produces elements in $\{-2, -1, 0, 1, 2\}$, thus it corresponds to a simple re-assignment of x to a different point on the four bit grid. See Figure 1 for an illustration of this decomposition.

This idea can be generalized to arbitrary power of two bit widths by sequentially doubling the precision of the quantized tensor through the addition of the, quantized, remaining residual error

$$x_q = x_2 + .pdfilon_4 + .pdfilon_8 + .pdfilon_{16} + .pdfilon_{32} \quad (4)$$

where each quantized residual is $.pdfilon_b = s_b \lfloor (x - x_{b/2})/s_b \rfloor$, with a step size $s_b = s_{b/2}/(2^{b/2} + 1)$, and previously quantized value $x_b = x_2 + \sum_{2 < j < b} .pdfilon_j$ for $b \in \{4, 8, 16, 32\}$. In this specific example, x_q will be quantized according to a 32-bit fixed point grid. Our lowest bit

width is 2-bit to allow for the representation of 0, e.g. in the case of padding in convolutional layers.

This decomposition is exact if the bit width doubles at each step. For a more general exposition, we refer the reader to the appendix.

Having obtained this decomposition, we then seek to learn the appropriate bit width. We introduce gating variables z_i , i.e. variables that take values in $\{0, 1\}$, for each residual error $.pdfilon_i$. More specifically, we can express the quantized value as

$$x_q = x_2 + z_4(.pdfilon_4 + z_8(.pdfilon_8 + z_{16}(.pdfilon_{16} + z_{32}.pdfilon_{32}))). \quad (5)$$

If one of the gates z_i takes the value of zero, it completely deactivates the addition of all of the higher bit width residuals, thus controlling the effective bit width of the quantized value x_q . But why stop there? We can take this a step further and consider pruning as quantization with a zero bit width. We can thus extend Eq. 5 as follows:

$$x_q = z_2(x_2 + z_4(.pdfilon_4 + z_8(.pdfilon_8 + z_{16}(.pdfilon_{16} + z_{32}.pdfilon_{32})))) \quad (6)$$

where now we also introduce a gate for the lowest bit width possible, z_2 . If that particular gate is switched off, then the input x is assigned the value of 0, thus quantized to 0-bit and pruned away. Armed with this modification, we can then perform, e.g., structured pruning by employing a separate quantizer of this form for each filter in a convolutional layer. To ensure that the elements of the tensor that survive the pruning will be quantized according to the same grid, we can share the gating variables for $b > 2$, along with the quantization grid step sizes.

2.2. Bayesian Bits

We showed in Eq. 6 that quantizing to a specific bit width can be seen as a gated addition of the quantized residual. We want to incorporate a principled regularizer for the gates, such that it encourages gate configurations that prefer efficient neural networks. We will derive such a regularizer through the lens of Bayesian inference; it will be given by a specific prior that favors low bit-width configurations.

For simplicity, let us assume that we are working on a supervised learning problem, where we are provided with a dataset of N i.i.d. input-output pairs $\mathcal{D} = \{(\mathbf{x}_i, y_i)\}_{i=1}^N$. Furthermore, let us assume that we have a neural network with parameters θ and a total of K quantizers that quantize up to 8-bit¹ with associated gates $\mathbf{z}_{1:K}$, where $\mathbf{z}_i = [z_{2i}, z_{4i}, z_{8i}]$. We can then use the neural network

¹This is just for simplifying the exposition and not a limitation of our method.

for the conditional distribution of the targets given the inputs, i.e. $p_\theta(\mathcal{D}|\mathbf{z}_{1:K}) = \prod_{i=1}^N p_\theta(y_i|x_i, \mathbf{z}_{1:K})$. Consider also positing a prior distribution (which we will discuss later) over the gates $p(\mathbf{z}_{1:K}) = \prod_k p(\mathbf{z}_k)$. We can then perform variational inference with an approximate posterior that has parameters ϕ , $q_\phi(\mathbf{z}_{1:K}) = \prod_k q(\mathbf{z}_k)$ by maximizing the following lower bound to the marginal likelihood $p_\theta(\mathcal{D})$ (Peterson, 1987; Hinton & Van Camp, 1993)

$$\mathcal{L}(\theta, \phi) = \mathbb{E}_{q_\phi(\mathbf{z}_{1:K})}[\log p_\theta(\mathcal{D}|\mathbf{z}_{1:K})] - \sum_k KL(q_\phi(\mathbf{z}_k)||p(\mathbf{z}_k)). \quad (7)$$

The first term can be understood as the ‘‘reconstruction’’ term, which aims to obtain good predictive performance for the targets given the inputs. The second term is the ‘‘complexity’’ term that, through the KL divergence, aims to regularize the variational posterior distribution to be as close as possible to the prior $p(\mathbf{z}_{1:K})$. Since each addition of the quantized residual doubles the bit width, let us assume that the gates $\mathbf{z}_{1:K}$ are binary; we either double the precision of each quantizer or we keep it the same. We can then set up an autoregressive prior and variational posterior distribution for the next bit configuration of each quantizer k , conditioned on the previous, as follows:

$$p(z_{2k}) = \text{Bern}(e^{-\lambda}), \quad q_\phi(z_{2k}) = \text{Bern}(\sigma(\phi_{2k})), \quad (8)$$

$$p(z_{4k}|z_{2k} = 1) = p(z_{8k}|z_{4k} = 1) = \text{Bern}(e^{-\lambda}), \quad (9)$$

$$q_\phi(z_{4k}|z_{2k} = 1) = \text{Bern}(\sigma(\phi_{4k})), \quad (10)$$

$$q_\phi(z_{8k}|z_{4k} = 1) = \text{Bern}(\sigma(\phi_{8k})) \quad (11)$$

$$p(z_{4k}|z_{2k} = 0) = p(z_{8k}|z_{4k} = 0) = \text{Bern}(0), \quad (12)$$

$$q(z_{4k}|z_{2k} = 0) = q(z_{8k}|z_{4k} = 0) = \text{Bern}(0), \quad (13)$$

where $e^{-\lambda}$ with $\lambda \geq 0$ is the prior probability of success and $\sigma(\phi_{ik})$ is the posterior probability of success with $\sigma(\cdot)$ being the sigmoid function and ϕ_{ik} the learnable parameters. Essentially, this structure encodes the fact that when the gate for e.g. 4-bit is ‘‘switched off’’, the gate for 8-bit will also be off, as it interacts with z_4 via the multiplication $z_4 z_8$. For brevity, we will refer to the variational distribution that conditions on an active previous bit as $q_\phi(z_{ik})$ instead of $q_\phi(z_{ik}|z_{i/2,k} = 1)$, since the ones conditioned on a previously inactive bit, $q_\phi(z_{ik}|z_{i/2,k} = 0)$, are fixed. We can then show that the KL divergence for each quantizer in the variational objective decomposes to

$$\begin{aligned} KL(q_\phi(\mathbf{z}_k)||p(\mathbf{z}_k)) &= KL(q_\phi(z_{2k})||p(z_{2k})) + \\ & q_\phi(z_{2k} = 1)KL(q_\phi(z_{4k})||p(z_{4k}|z_{2k} = 1)) + \\ & q_\phi(z_{2k} = 1)q_\phi(z_{4k} = 1)KL(q_\phi(z_{8k})||p(z_{8k}|z_{4k} = 1)) \end{aligned} \quad (14)$$

We can see that the posterior inclusion probabilities of the lower bit widths downscale the KL divergence of the higher

bit widths. This is important, as the gates for the higher order bit widths can only contribute to the log-likelihood of the data when the lower ones are active due to their multiplicative interaction. Therefore, the KL divergence at Eq. 14 prevents the over-regularization that would have happened if we had assumed fully factorized distributions.

2.3. A simple approximation for learning the bit width

So far we have kept the prior as an arbitrary Bernoulli with a specific form for the probability of inclusion, $e^{-\lambda}$. How can we then enforce that the variational posterior will “prune away” as many gates as possible? The straightforward answer would be by choosing large values for λ ; for example, if we are interested in networks that have low computational complexity, we can set λ proportional to the Bit Operation (BOP) count contribution of the particular object that is to be quantized. By writing out the KL divergence with this specific prior for a given KL term, we will have that

$$KL(q_\phi(z_{ik})||p(z_{ik})) = -H[q_\phi] + \lambda q(z_{ik} = 1) - \log(1 - e^{-\lambda})(1 - q(z_{ik} = 1)), \quad (15)$$

where $H[q_\phi]$ corresponds to the entropy of the variational posterior $q_\phi(z_{ik})$. Now, under the assumption that λ is sufficiently large, we have that $(1 - e^{-\lambda}) \approx 1$, thus the third term of the r.h.s. vanishes. As a result, we have that

$$KL(q_\phi(z_{ik})||p(z_{ik})) \approx -H[q_\phi] + \lambda q_\phi(z_{ik} = 1). \quad (16)$$

Now, let us assume that we want to optimize the objective of Eq. 7; we can rescale it, without changing the optima, according to the size of the dataset, N , as follows:

$$\mathcal{L}(\theta, \phi) = \mathbb{E}_{q_\phi(\mathbf{z}_{1:K})} \left[\frac{1}{N} \log p_\theta(\mathcal{D}|\mathbf{z}_{1:K}) \right] - \frac{1}{N} \sum_k KL(q_\phi(\mathbf{z}_k)||p(\mathbf{z}_k)) \quad (17)$$

where we now optimize for the average log-likelihood and similarly downscale the KL divergence. In this case the individual KL divergences will be

$$\frac{1}{N} KL(q_\phi(z_{ik})||p(z_{ik})) \approx -\frac{1}{N} H[q_\phi] + \frac{\lambda}{N} q_\phi(z_{ik} = 1). \quad (18)$$

For large datasets the contribution of the entropy term will then be negligible. Equivalently, we can consider doing MAP estimation on the objective of Eq. 7, which corresponds to simply ignoring the entropy terms of the variational bound. Now by reparametrizing λ as $\lambda = N\lambda'$ the second term of the r.h.s. will survive irrespective of the size of the dataset and the complexity cost will be

$$\frac{1}{N} KL(q_\phi(z_{ik})||p(z_{ik})) \approx \lambda' q_\phi(z_{ik} = 1). \quad (19)$$

Putting everything together, we arrive at a simple and intuitive objective function

$$\mathcal{F}(\theta, \phi) := \mathbb{E}_{q_\phi(\mathbf{z}_{1:K})} \left[\frac{1}{N} \log p_\theta(\mathcal{D}|\mathbf{z}_{1:K}) \right] - \lambda' \sum_k \sum_{i \in B} \prod_{j \in B}^{j \leq i} q_\phi(z_{jk} = 1), \quad (20)$$

where B corresponds to the available bit widths of the quantizers, e.g. $B = \{2, 4, 8, 16, 32\}$. This objective can be understood as penalizing the probability of including the set of parameters associated with each quantizer and additional bits of precision assigned to them.

It is interesting to see that the overall objective that we arrive at is similar to the stochastic version of the L_0 regularizer of (Louizos et al., 2018). By using the fact that

$$\sum_{i \in B} \prod_{j \in B}^{j \leq i} q_\phi(z_{jk} = 1) = \mathbb{E}_{q_\phi(\mathbf{z}_k)} \left[\sum_{i \in B} \prod_{j \in B}^{j \leq i} \mathbb{I}[z_{jk} \neq 0] \right], \quad (21)$$

we can rewrite Eq. 20 as follows:

$$\mathcal{F}(\theta, \phi) := \mathbb{E}_{q_\phi(\mathbf{z}_{1:K})} \left[\frac{1}{N} \log p_\theta(\mathcal{D}|\mathbf{z}_{1:K}) - \lambda' \sum_k \sum_{i \in B} \prod_{j \in B}^{j \leq i} \mathbb{I}[z_{jk} \neq 0] \right]. \quad (22)$$

Now by assuming that the parameters will not be quantized, i.e. $z_4 = z_8 = z_{16} = z_{32} = 1$ the objective becomes

$$\mathbb{E}_{q_\phi(\mathbf{z}_{2,1:K})} \left[\frac{1}{N} \log p_\theta(\mathcal{D}|\mathbf{z}_{2,1:K}) - \lambda' |B| \sum_k \mathbb{I}[z_{2k} \neq 0] \right], \quad (23)$$

which corresponds to regularizing with a specific strength the expected L_0 norm of the vector that determines the group of parameters that will be included in the model.

2.4. Practical considerations

The final objective we arrived at in Eq. 20 requires us to compute an expectation of the log-likelihood with respect to the stochastic gates. For a moderate amount of gates, this can be expensive to compute. One straightforward way to avoid it is to approximate the expectation with a Monte Carlo average by sampling from $q_\phi(\mathbf{z}_{1:K})$. While this is certainly easier to do, we would still need to compute the gradients of ϕ through the sampling process with the reparametrization trick (Kingma & Welling, 2014; Rezende et al., 2014). Unfortunately, this is not possible in this case, as sampling

from a Bernoulli distribution is a non-differentiable operation. However, by exploiting the alternative formulation of the objective presented in Eq. 22, we can replace the Bernoulli distributions for $q_\phi(\mathbf{z}_{1:K})$ with hard concrete relaxations (Louizos et al., 2018) $r_\phi(\mathbf{z}_{1:K})$, which allow for gradient-based optimization. More specifically, the hard concrete distribution has the following sampling process:

$$u_{jk} \sim U[0, 1], \quad g_{jk} = \log \frac{u_{jk}}{1 - u_{jk}}, \quad s_{jk} = \sigma \left(\frac{g_{jk} + \phi_{jk}}{b} \right) \\ z_{jk} = \min(1, \max(0, s_{jk}(\zeta - \gamma) + \gamma)) \quad (24)$$

where $\sigma(\cdot)$ corresponds to the sigmoid function, b is a temperature hyperparameter and ζ, γ are hyperparameters that ensure z has support for exact 0, 1. Essentially, it corresponds to a mixture distribution that has three components: one that corresponds to zero, one that corresponds to one and one that produces values in $(0, 1)$. Under this relaxation, the objective in Eq. 22 will be converted to

$$\mathcal{F}(\theta, \phi) := \mathbb{E}_{r_\phi(\mathbf{z}_{1:K})} \left[\frac{1}{N} \log p_\theta(\mathcal{D} | \mathbf{z}_{1:K}) \right] - \\ \lambda' \sum_k \sum_{i \in B} \prod_{j \leq i} R_\phi(z_{jk} > 0). \quad (25)$$

where $R_\phi(\cdot)$ corresponds to complementary cumulative distribution function, i.e. $1 - R_\phi(\cdot)$ is the cumulative distribution function (CDF), of the density $r_\phi(z)$ induced by the sampling process described at Eq. 24. The $R_\phi(z_{jk} > 0)$ now corresponds to the probability of activating the gate z_{jk} and has the following simple form

$$R_\phi(z_i > 0) = \sigma \left(\phi - b \log \frac{-\gamma}{\zeta} \right). \quad (26)$$

It is now easy to optimize the objective in Eq. 25 using gradient descent with a Monte Carlo estimate of the expectation and the reparametrization trick. At test time, the authors of Louizos et al. (2018) propose a deterministic variant of Eq. 24, where the noise is switched off. As that can result into gates that are not exactly 0 or 1, thus not exactly corresponding to doubling the bits of precision, we take an alternative approach. We prune a gate whenever the probability of exact zero under $r_\phi(z)$ exceeds a threshold t , otherwise we set it to 1

$$z = \mathbb{I} \left[\sigma \left(\beta \log \left(-\frac{\gamma}{\zeta} \right) - \phi \right) < t \right], \quad (27)$$

where we set $t = 0.34$. This threshold value corresponds to the case when the probability of the mixture component corresponding to exact zero is higher than the other two.

For the decomposition of the quantization operation that we previously described, we need the inputs to be constrained

within the quantization grid $[\alpha, \beta]$. A simple way to do this would be to clip the inputs before pushing them through the quantizer. For this clipping we will use PACT (Choi et al., 2018), which in our case clips the inputs according to

$$\text{clip}(x; \alpha, \beta) = \beta - \text{ReLU}(\beta - \alpha - \text{ReLU}(x - \alpha)) \quad (28)$$

where β, α can be trainable parameters. In practice we only learn β as we set α to zero for unsigned quantization (e.g. for ReLU activations), and for signed quantization we set $\alpha = -\beta$. We also found it beneficial to subtract a small padding from β via $(1 - 10^{-7})\beta$ before we use it at Eq. 28. This ensures that we avoid the corner case in which a value of exactly β is rounded up to an invalid grid point. The step size of the initial grid is then parametrized as $s_2 = \frac{\beta - \alpha}{2^2 - 1}$.

Finally, for the gradients of the parameters θ , weights and biases of the network, we follow the standard practice and employ the straight-through estimator (STE) (Bengio et al., 2013) for the rounding operation, i.e., we perform the rounding in the forward pass but ignore it in the backward pass by assuming that the operation is the identity.

3. Related work

The method most closely related to our work is Differential Quantization (DQ) (Uhlich et al., 2020). In this method, the quantization range and scale are learned from data jointly with the model weights, from which the bit width can be inferred. However, for hardware-friendly application of this method, the learned bit widths must be rounded up to the nearest power-of-two. As a result, hypothetical efficiency gains will likely not be met in reality.

Several other methods for finding mixed precision configurations have been introduced in the literature. Dong et al. (2019b) and follow-up work Dong et al. (2019a) use respectively the largest eigenvalue and the trace of the Hessian to determine a layer’s sensitivity to perturbations. The intuition is that strong curvature at the loss minimum implies that small changes to the weights will have a big impact on the loss. Similarly to this work, Louizos et al. (2017) takes a Bayesian approach and determines the bit width for each weight tensor through heuristic based on the weight uncertainty in the variational posterior. The drawback, similarly to Uhlich et al. (2020), of such an approach is that there is no inherent control over the resulting bit widths.

Wu et al. (2019) frames the mixed precision search problem as an architecture search. For each layer in their network, the authors maintain a separate weight tensor for each bit width under consideration. A stochastic version of DARTS (Liu et al., 2018) is then used to learn the optimal bit width setting jointly with the network’s weights.

Wang et al. (2019) model the assignment of bit widths as a

reinforcement learning problem. Their agent’s observation consists of properties of the current layer, and its action space is the possible bit widths for a layer. The agent receives the validation set accuracy after a short period of fine-tuning as a reward. Besides the reward, the agent receives direct hardware feedback from a target device, which is used to constrain the search space. This feedback allows the agent to adapt to specific hardware directly, instead of relying on proxy measures.

Learning the scale along with the model parameters for a fixed bit width network was independently introduced by (Esser et al., 2020) and Jain et al. (2019). Both papers redefine the quantization operation to expose the scale parameter to the learning process, which is then optimized jointly with the network’s parameters. Similarly, Choi et al. (2018) reformulate the clipping operation such that the range of activations in a network can be learned from data, leading to activation ranges that are more amenable to quantization.

The recursive decomposition introduced in this paper shares similarities with previous work on residual vector quantization (Chen et al., 2010), in which the residual error of vectors quantized using K-means is itself (recursively) quantized. Gong et al. (2015) apply this method to neural network weight compression: the size of a network can be significantly reduced by only storing the centroids of K-means quantized vectors. Our decomposition also shares similarities with Li et al. (2017b). A crucial difference between their decomposition and ours is that in the decomposition in Li et al. (2017b) the sum of quantized residual tensors does not in itself yield a valid fixed-point tensor.

4. Experiments

To evaluate our proposed method we conduct experiments on image classification tasks. In every model, we quantized all of the weights and activations (besides the output logits) and handled the batch normalization layers as discussed in Krishnamoorthi (2018). The parameters of the gates were initialized to a large value so that initially the model is using its full 32-bit capacity without pruning.

We evaluate our method on two axes, classification accuracy of the final model on the test set and the model’s overall complexity in terms of bit operations (BOPs). The BOP count for each layer l is estimated with the following formula:

$$\text{BOPs}(l) = \text{MACs}(l)b_w b_a \quad (29)$$

where b_w, b_a correspond to the bit width of the weights and input activations, respectively, and $\text{MACs}(l)$ corresponds to the MAC count of that layer. We refer the reader to the appendix for details on how sparsity affects a layer’s MAC count. Finally, we set the regularization strength for each gate z_{jk} to be $\mu\lambda'_{jk}$, where

λ'_{jk} is proportional to the BOP count corresponding to the bit width j and the MAC count of the layer l_k that the quantizer k operates on. Specifically, we set $\lambda'_{jk} = b_j \text{MACs}(l_k) / \max([\text{MACs}(1), \dots, \text{MACs}(L)])$, where b_j is the bit width that gate j controls and L corresponds to the total number of layers. For activation quantizers, we use the MAC count of the layer into which the activation is fed. We then perform hyperparameter tuning for the global scaling factor μ . Unless mentioned otherwise, the range parameter β is initialized to the maximum of either the weight tensor or the activation values on the first batch and was trained jointly with the other parameters. We perform group sparsity on the output channels / units for the weight tensors (by enabling the zero bit option) but for the activations we only perform quantization (i.e. set $z_2 = 1$ always), as pruning an output channel of the weight tensor corresponds to pruning that specific activation. It is worth noting that such a configuration for the regularization strength is certainly not the only choice; we can also encourage low memory networks by e.g. using the regularizer from (Uhlich et al., 2020) or even allow for hardware aware pruning and quantization by using e.g. a hardware simulator.

We then compare our proposed approach to literature that considers both static as well as mixed precision architectures. If BOP counts for a specific model are not provided by the original papers, we perform our own BOP computations. The assumptions made in doing so can be found in the appendix. We note that the bit widths of all quantizers in our network are learned, contrary to common practice in quantization literature (e.g. Choi et al. (2018); Wu et al. (2019) which k.pdf the first and last layers of the networks in full precision or a higher bit width.

While our proposed method facilitates an end-to-end gradient based optimization for pruning and quantization, in practical applications, one might not have access to large datasets and the appropriate compute. For this reason, we also perform a series of experiments in which only the quantization parameters are updated on a pre-trained model, using a small dataset and few epochs of training on a consumer-grade GPU. As a result, Bayesian Bits can serve as a method in-between ‘push-button’ post-training methods that do not require backpropagation, such as Nagel et al. (2019), and methods in which the full model is fine-tuned, due to the relatively minor data and compute requirements.

During training, the optimization of the gates according to Eq. 6 requires us to essentially keep $|B|$ copies of the inputs to the quantizer, i.e. weight tensors and activation feature maps, where $|B|$ is the number of possible bit widths that we allow. This can be problematic, memory wise, for large neural networks during backpropagation. To circumvent this issue, we employ checkpointing (Chen et al., 2016); after we use the quantized residuals in the forward pass we

discard them and save the input to the quantizer. In the backward pass we then recompute the quantized residuals according to the quantizer input, since they are part of the gradient. Notice that this is not an issue during inference time, as we can directly quantize to the learned bit width.

4.1. Toy experiments on MNIST & CIFAR 10

For the first experiment, we considered the toy tasks of MNIST and CIFAR 10 classification using a LeNet-5 and a VGG-7 model, respectively, commonly employed in the quantization literature, e.g., Li et al. (2017a). We provide the experimental details in the appendix. For the VGG experiment, we also implemented the DQ method from Uhlich et al. (2020) with a BOP regularizer instead of a memory one so that it can directly be compared to Bayesian Bits. We considered two cases for DQ: one where the bit widths are unconstrained and one where we round up to the nearest bit width that is a power of two (DQ-restricted).

Table 1. Results on the MNIST task, mean and stderr over 3 runs. We compare against TWN (Li et al., 2017a), LR-Net (Shayer et al., 2017), RQ (Louizos et al., 2019) and WAGE (Wu et al., 2018). LR-Net has the last layer in full precision.

Method	# bits W/A	Acc. (%)	Rel. GBOPs (%)
Full precision	32/32	99.36	100
TWN	2/32	99.35	5.74
LR-Net	1/32	99.47	2.99
RQ	2/2	99.37	0.52
WAGE	2/8	99.60	1.56
Bayesian Bits $\mu = 0.1$	Mixed	99.30±0.03	0.36±0.01

Table 2. Results on the CIFAR 10 task, mean and stderr over 3 runs. We additionally compare against DQ (Uhlich et al., 2020). LR-Net has the last layer in full precision.

Method	# bits W/A	Acc. (%)	Rel. GBOPs (%)
Full precision	32/32	93.05	100
TWN	2/32	92.56	6.22
LR-Net	1/32	93.18	3.11
RQ	8/8	93.30	6.25
RQ	4/4	92.04	1.57
WAGE	2/8	93.22	1.56
DQ	Mixed	91.59	0.48
DQ - restricted	Mixed	91.59	0.54
Bayesian Bits $\mu = 0.01$	Mixed	93.23±0.10	0.51±0.03
Bayesian Bits $\mu = 0.1$	Mixed	91.96±0.04	0.29±0.00

As we can see from the results of Tables 1,5, our proposed method provides better trade-offs between the computational complexity of the resulting architecture and the final accuracy on the test set. On MNIST we can maintain similar accuracy to the prior art while reducing the amount of GBOPs even further. On CIFAR 10 we get an error that is similar to WAGE (Wu et al., 2018), while using only 35% of its GBOPs. By increasing the regularization strength, we take a hit of approximately 1% extra test set error. However, we can reduce the amount of GBOPs even further, using

only 0.29% the BOPs of the full precision model.

We plot the learned sparsity and bit widths for our models in Figure 2. There we observe that in the aggressive regularization regimes, Bayesian Bits quantizes almost all of the tensors to 2-bit, but usually k.pdf the first and last layers to higher bit-precision, which is in line with common practices of the quantization literature. In the case of moderate regularization at VGG, we observe that Bayesian Bits hardly prunes, it removed 2 channels at the last 256 output convolutional layer and 8 channels at the penultimate weight tensor, and prefers to keep most weight tensors at 2-bit whereas the activations range from 2-bit to 16-bit.

4.2. Experiments on Imagenet

For the experiments on Imagenet we used the ResNet18 architecture (He et al., 2016) commonly employed in the quantization literature (Jacob et al., 2018; Louizos et al., 2019; Choi et al., 2018). We started from the pretrained model from the PyTorch (Paszke et al., 2019) model zoo, which we fine-tuned for 30 epochs using Bayesian Bits. The experimental details can similarly be found in the appendix.

As we can observe from the results in Figure 3 (the corresponding table can be found in the appendix), Bayesian Bits can find different trade-offs on the accuracy vs. efficiency curve by changing the regularization strength. In general, we observe that for small amounts of regularization Bayesian Bits does not prune, but instead prefers to quantize the network. In this case, a small decrease in top-1 accuracy (-0.6%) decreases the BOP count to about 2% of BOP count of the full precision baseline. In the case of moderate regularization, there is an decrease of about 2% in top-1 accuracy, but a reduction of the BOP count to around 1.4% of the full precision baseline. For an aggressive regularization of $\mu = 0.2$ we observe an decrease in the top-1 accuracy of approximately 6% compared to the baseline model, but the BOP count are only 0.75% of the original model. We provide the tables of the results in the appendix along with visualizations of the learned ResNet18 architectures in this setting. Overall, we observe that Bayesian Bits provides better trade-offs between accuracy and efficiency compared to the baselines.

There are several works of note to which we cannot directly compare our results. Wang et al. (2019) only present Imagenet results on ResNet50 (He et al., 2016) and MobileNet (Sandler et al., 2018) architectures. Dong et al. (2019b;a) and Wu et al. (2019) do present Imagenet results on ResNet18, but do not provide the mixed precision configuration for their reported results. While Wu et al. (2019) provide the BOP count of the resulting ResNet18 network, it is not mentioned whether the fact that the first and last layers are in full precision is taken into account in determining the compute reduction. Furthermore, they include a 3-bit

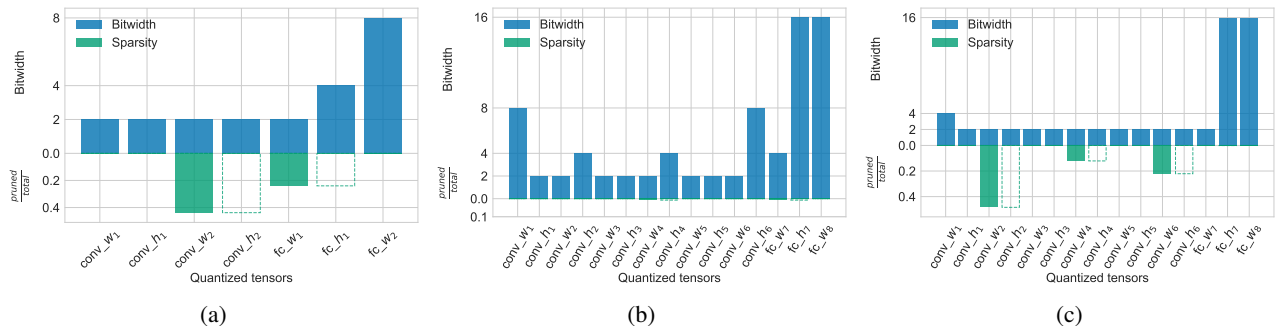


Figure 2. Learned LeNet-5 and VGG architectures. (a) Illustrates the bit-allocation and sparsity levels for the LeNet-5 whereas (b) illustrates the bit-allocation and sparsity levels for the best performing VGG, accuracy wise. (c) Illustrates a VGG model trained with more aggressive regularization, resulting into less BOPs and more quantization / sparsity. With the dashed lines we show the implied sparsity on the activations due to the sparsity in the (preceding) weight tensors.

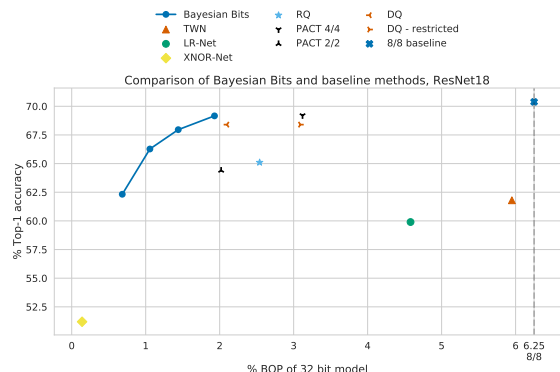


Figure 3. Imagenet Results. Bayesian Bits Imagenet validation accuracy on ResNet18 for $\mu \in \{0.03, 0.05, 0.07, 0.2\}$. Bayesian Bits (No Pruning) uses $\mu = 0.03$. The Bayesian Bits results show the mean over 3 training runs, except for $\mu = 0.2$ which only has 2 runs. DQ results are produced by us, all other results are taken from the respective papers. The BOP count per model is presented in the appendix. In this plot we additionally compare to XNOR-Net (Rastegari et al., 2016) and PACT (Choi et al., 2018).

configuration in their search space, which is not efficiently implemented in hardware.

Post-training mixed precision In this experiment, we evaluate the ability of our method to find sensible mixed precision settings by learning the values of the gates on a pre-trained model, while keeping the weights fixed. To show that our method can achieve good results on a small dataset, we use a subsampled version of Imagenet with four images per class. We find mixed precision settings that trade off accuracy with efficiency by modifying the regularization strength. For each different hyperparameter setting, optimization is run on the small dataset for 30 epochs. On a consumer-grade NVIDIA GeForce GTX 2080Ti GPU this optimization procedure takes about 50 minutes. We run a second set of experiments in which we jointly optimize the scale parameters β with the gate parameters, as this introduces negligible extra cost.

We compare our method against an iterative baseline method, which consists of two phases: In the first phase, the quantization sensitivity of each of the N (weight or activation) tensors in the network is assessed by quantizing each tensor to the B low bit widths under consideration, while keeping the rest of the network in full precision, and measuring the increase in error on the same small training set. In the second phase the quantizers and bit widths are sorted in increasing order of quantization sensitivity. The network is then iteratively quantized according to this order. At each new quantization step the error on a validation set is measured. The baseline method requires NB evaluations of the small training set and NB evaluations of the validation set, as opposed to fixed 30 epochs on the small training set for Bayesian Bits.

Figure 4 compares the Pareto front of our method with that of the baseline method and an 8/8 fixed bit width baseline. More detailed results can be found in the appendix. We see that optimizing the gates alone beats the baseline for high prediction accuracies. Furthermore, optimizing the scales jointly with the gates gives a significant boost, outperforming all baselines everywhere. Note that there is no efficient way to optimize the β parameters in the baseline method.

5. Conclusion

In this work we introduced Bayesian Bits, a practical method that can effectively learn appropriate bit widths for efficient neural networks in an end-to-end fashion through gradient descent. It is realized via a novel decomposition of the quantization operation that sequentially considers additional bits via a gated addition of quantized residuals. We show how to optimize said gates while incorporating principled regularizers through the lens of sparsifying priors for Bayesian inference. We further show that such an approach provides a unifying view of pruning and quantization, is hardware friendly, and, under some assumptions, corresponds to an L_0 regularization for the learnable gates. Experimentally, we demonstrated that our proposed approach finds more

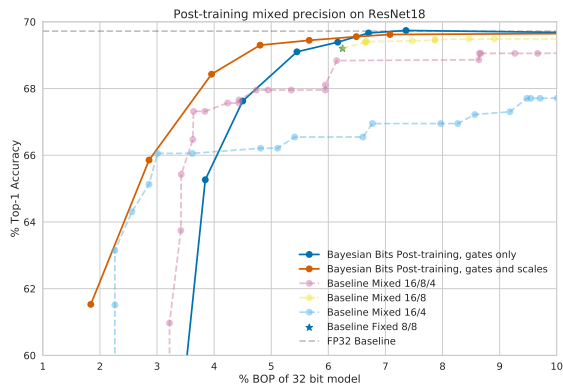


Figure 4. Pareto fronts. Pareto fronts of Bayesian Bits post-training and the baseline method, as well as a fixed (post-training) 8/8 baseline. For our method mean results over 3 runs are plotted with solid lines.

efficient networks than prior art.

References

- Bengio, Y., Léonard, N., and Courville, A. Estimating or propagating gradients through stochastic neurons for conditional computation. *arXiv preprint arXiv:1308.3432*, 2013.
- Chen, T., Xu, B., Zhang, C., and Guestrin, C. Training deep nets with sublinear memory cost. *arXiv preprint arXiv:1604.06174*, 2016.
- Chen, Y., Guan, T., and Wang, C. Approximate nearest neighbor search by residual vector quantization. *Sensors*, 10(12):11259–11273, 2010.
- Choi, J., Wang, Z., Venkataramani, S., Chuang, P. I.-J., Srinivasan, V., and Gopalakrishnan, K. Pact: Parameterized clipping activation for quantized neural networks. *arXiv preprint arXiv:1805.06085*, 2018.
- Dong, Z., Yao, Z., Cai, Y., Arfeen, D., Gholami, A., Mahoney, M. W., and Keutzer, K. Hawq-v2: Hessian aware trace-weighted quantization of neural networks. *arXiv preprint arXiv:1911.03852*, 2019a.
- Dong, Z., Yao, Z., Gholami, A., Mahoney, M. W., and Keutzer, K. HAWQ: hessian aware quantization of neural networks with mixed-precision. *International Conference on Computer Vision (ICCV)*, 2019b.
- Esser, S. K., McKinstry, J. L., Bablani, D., Appuswamy, R., and Modha, D. S. Learned step size quantization. *International Conference on Learning Representations (ICLR)*, 2020.
- Gong, Y., Liu, L., Yang, M., and Bourdev, L. Compressing deep convolutional networks using vector quantization. *International Conference on Learning Representations (ICLR)*, 2015.
- He, K., Zhang, X., Ren, S., and Sun, J. Deep residual learning for image recognition. *Conference on Computer Vision and Pattern Recognition, CVPR*, 2016.
- Hinton, G. E. and Van Camp, D. Keeping the neural networks simple by minimizing the description length of the weights. In *Conference on Computational learning theory (COLT)*, 1993.
- Ignatov, A., Timofte, R., Kulik, A., Yang, S., Wang, K., Baum, F., Wu, M., Xu, L., and Van Gool, L. Ai benchmark: All about deep learning on smartphones in 2019. *International Conference on Computer Vision (ICCV) Workshops*, 2019.
- Jacob, B., Kligys, S., Chen, B., Zhu, M., Tang, M., Howard, A., Adam, H., and Kalenichenko, D. Quantization and training of neural networks for efficient integer-arithmetic-only inference. *Conference on Computer Vision and Pattern Recognition (CVPR)*, 2018.
- Jain, S. R., Gural, A., Wu, M., and Dick, C. Trained uniform quantization for accurate and efficient neural network inference on fixed-point hardware. *arxiv preprint arxiv:1903.08066*, 2019.
- Kingma, D. P. and Ba, J. Adam: A method for stochastic optimization. *International Conference on Learning Representations (ICLR)*, 2015.
- Kingma, D. P. and Welling, M. Auto-encoding variational bayes. *International Conference on Learning Representations (ICLR)*, 2014.
- Krishnamoorthi, R. Quantizing deep convolutional networks for efficient inference: A whitepaper. *arXiv preprint arXiv:1806.08342*, 2018.
- Kuzmin, A., Nagel, M., Pitre, S., Pendyam, S., Blankevoort, T., and Welling, M. Taxonomy and evaluation of structured compression of convolutional neural networks. *arXiv preprint arXiv:1912.09802*, 2019.
- Li, F., Zhang, B., and Liu, B. Ternary weight networks. *International Conference on Learning Representations (ICLR)*, 2017a.
- Li, Z., Ni, B., Zhang, W., Yang, X., and Gao, W. Performance guaranteed network acceleration via high-order residual quantization. In *Proceedings of the IEEE International Conference on Computer Vision*, pp. 2584–2592, 2017b.
- Liu, H., Simonyan, K., and Yang, Y. Darts: Differentiable architecture search. *International Conference on Learning Representations (ICLR)*, 2018.

- Louizos, C., Ullrich, K., and Welling, M. Bayesian compression for deep learning. *Neural Information Processing Systems (NeurIPS)*, 2017.
- Louizos, C., Welling, M., and Kingma, D. P. Learning sparse neural networks through l_0 regularization. *International Conference on Learning Representations (ICLR)*, 2018.
- Louizos, C., Reisser, M., Blankevoort, T., Gavves, E., and Welling, M. Relaxed quantization for discretized neural networks. In *International Conference on Learning Representations (ICLR)*, 2019.
- Moons, B., Uytterhoeven, R., Dehaene, W., and Verhelst, M. 14.5 envision: A 0.26-to-10tops/w subword-parallel dynamic-voltage-accuracy-frequency-scalable convolutional neural network processor in 28nm fdsoi. In *2017 IEEE International Solid-State Circuits Conference (ISSCC)*, pp. 246–247. IEEE, 2017.
- Nagel, M., van Baalen, M., Blankevoort, T., and Welling, M. Data-free quantization through weight equalization and bias correction. *International Conference on Computer Vision (ICCV)*, 2019.
- Paszke, A., Gross, S., Massa, F., Lerer, A., Bradbury, J., Chanan, G., Killeen, T., Lin, Z., Gimelshein, N., Antiga, L., Desmaison, A., Kopf, A., Yang, E., DeVito, Z., Raison, M., Tejani, A., Chilamkurthy, S., Steiner, B., Fang, L., Bai, J., and Chintala, S. Pytorch: An imperative style, high-performance deep learning library. In *Neural Information Processing Systems (NeurIPS)*. 2019.
- Peterson, C. A mean field theory learning algorithm for neural networks. *Complex systems*, 1:995–1019, 1987.
- Rastegari, M., Ordonez, V., Redmon, J., and Farhadi, A. Xnor-net: Imagenet classification using binary convolutional neural networks. In *European Conference on Computer Vision*, pp. 525–542. Springer, 2016.
- Rezende, D. J., Mohamed, S., and Wierstra, D. Stochastic backpropagation and approximate inference in deep generative models. *International Conference on Machine Learning (ICML)*, 2014.
- Sandler, M., Howard, A., Zhu, M., Zhmoginov, A., and Chen, L.-C. Mobilenetv2: Inverted residuals and linear bottlenecks. In *Conference on Computer Vision and Pattern Recognition (CVPR)*, June 2018.
- Shayer, O., Levi, D., and Fetaya, E. Learning discrete weights using the local reparameterization trick. *International Conference on Learning Representations (ICLR)*, 2017.
- Uhlich, S., Mauch, L., Yoshiyama, K., Cardinaux, F., García, J. A., Tiedemann, S., Kemp, T., and Nakamura, A. Mixed precision dnns: All you need is a good parametrization. *International Conference on Learning Representations (ICLR)*, 2020.
- Wang, K., Liu, Z., Lin, Y., Lin, J., and Han, S. Haq: Hardware-aware automated quantization with mixed precision. In *Conference on Computer Vision and Pattern Recognition (CVPR)*, 2019.
- Wu, B., Wang, Y., Zhang, P., Tian, Y., Vajda, P., and Keutzer, K. Mixed precision quantization of convnets via differentiable neural architecture search. *International Conference on Learning Representations (ICLR)*, 2019.
- Wu, S., Li, G., Chen, F., and Shi, L. Training and inference with integers in deep neural networks. *International Conference on Learning Representations (ICLR)*, 2018.

Bayesian Bits: Unifying Quantization and Pruning

Supplementary Material

A. Experimental details

The LeNet-5 model is realized as 32C5 - MP2 - 64C5 - MP2 - 512FC - Softmax, whereas the VGG is realized as 2x(128C3) - MP2 - 2x(256C3) - MP2 - 2x(512C3) - MP2 - 1024FC - Softmax. The notations is as follows: 128C3 corresponds to a convolutional layer of 128 feature maps with 3x3 kernels, MP2 corresponds to max-pooling with 2x2 kernels and a stride of 2, 1024FC corresponds to a fully connected layer with 1024 hidden units and Softmax corresponds to the classifier. Both models used ReLU nonlinearities, whereas for the VGG we also employed Batch-normalization for every layer except the last one. The weights, biases, gates, and ranges were optimized with Adam (Kingma & Ba, 2015) using the default hyper-parameters for 100 epochs on MNIST, 300 epochs on CIFAR 10 and during the last 1/3 epochs we linearly decayed the learning rate to zero. For CIFAR 10, we also performed standard data augmentation: random horizontal flips, random crops of 4 pixel padded images, and channel standardization. For the test images, we only performed channel standardization.

For the ResNet18 we used SGD with a learning rate of 3e-3 and Nesterov momentum of 0.9 for the network parameters and used Adam with the default hyperparameters for the optimization of the gate parameters and ranges. The learning rates for all of the optimizers were decayed by a factor of 10 after every 10 epochs. We did not employ any weight decay and used a batch-size of 384 distributed across four Tesla V100 GPUs.

B. MAC and BOP computation for sparsified networks

Since the sparsification only affects a layer’s MAC count and not its bit width, the equation for computing the BOP count,

$$\text{BOPs}(l) = \text{MACs}(l)b_w b_a, \quad (30)$$

holds for sparsified networks as well. However, it is insightful to see how sparsity affects a layer’s MAC count.

The MAC count of a convolutional layer can be derived as follows. For each output pixel in a feature map we know that $W_f \times W_h \times B$ computations were performed, where W_f and W_h are the filter width and height, and B is the convolutional block size (e.g. for dense convolutions B

is equal to the number of input channels, for depthwise separable convolutions B is equal to 1). There are $C_o \times W \times H$ output pixels, where C_o is the number of output channels, and W and H are the width and height of the output map. Henceforth we only consider dense convolutional layers, i.e. layers where $B = C_i$ where C_i is the number of input channels. Thus, the MAC count of a convolutional layer l can be computed as $\text{MACs}(l) = C_o \times W \times H \times C_i \times W_f \times H_f$. Note that in this formulation, no special care needs to be taken in considering padding, stride, or dilations.

As stated earlier, pruning output channels of layer $l - 1$ corresponds to pruning the associated activations, which in turn corresponds to pruning input channels of layer l . If we assume that $C_{i'}$ output channels are maintained in layer $l - 1$, and $C_{o'}$ output channels are maintained in layer l , the pruned MAC count can be computed as:

$$\text{MACs}_{\text{pruned}}(l) = p_i C_i p_o C_o W H W_f H_f \quad (31)$$

$$= p_i p_o \text{MACs}(l) \quad (32)$$

where $p_i = C_{i'}/C_i$, $p_o = C_{o'}/C_o$, and $\text{MACs}(l)$ is used to denote the MAC count of the unpruned layer. As a result, if we know the input and output pruning ratios p_i and p_o , the BOP count can be computed without recomputing the MAC count for the pruned layers with a slight modification of equation 30:

$$\text{BOPs}_{\text{pruned}}(l) = \text{MACs}_{\text{pruned}}(l)b_w b_a \quad (33)$$

$$= p_i p_o \text{MACs}(l)b_w b_a \quad (34)$$

B.1. ResNet18 MAC count computation

To compute the BOP count for ResNet18 models, we need to be careful with our application of equation 34, due to the presence of residual connections: to turn off an input channel at the input of a residual block, it must be turned off both in the output of the previous block as well as in the residual connection. We circumvent this issue by only considering p_i for the inputs of the second convolutional layer in each of the residual blocks, where there is no residual connection. Elsewhere, p_i is always assumed to be 1. Output pruning is treated as in any other network, since the removal of output channels always leads to reduced MAC

count. Thus, the BOP counts reported for ResNet18 models must be interpreted as an upper bound; the real BOP count may be lower.

B.2. ResNet18 regularization

In ResNet architectures, the presence of downsample layers means that certain quantized activation tensors feed into two multiple convolution operations, i.e. the downsample layer and the input layer of the corresponding block. As a result, we need to slightly modify the computation of λ'_{jk} as introduced in Section 4 for these activation quantizers. For an activation quantizer k for which this is the case, we compute λ'_{jk} as follows:

$$\lambda'_{jk} = b_j \frac{(\text{MACs}(l_d) + \text{MACs}(l_c))}{\max([\text{MACs}(1) \dots, \text{MACs}(L)])} \quad (35)$$

where l_d and l_c denote the downsample layer and the first convolutional layer in the corresponding block respectively.

C. Decomposed quantization for non-doubling bit widths

Consider the general case of moving from bit width a to bit width b , where $0 < a < b$, for a given range $[\alpha, \beta]$. Using the equation of section 2.1, i.e. $s_b = s_a/2^{b-a} - 1$ yields a value of $(\beta - \alpha)/N$, where $N = 2^b + 2^a - 2^{b-a} - 1$. If $b = 2a$ then this simplifies to $N = 2^b - 1$, which is the desired result. However, if $b \neq 2a$ then there are two cases to distinguish:

1. $b > 2a$, in this case we can write $N = 2^{2a+c} + 2^a - 2^{a+c} - 1$, where $c = b - 2a$. There are $2^{a+c} - 2^a$ bins more than desired in the range.
2. $b < 2a$, in this case we can write $N = 2^{2a-c} + 2^a - 2^{a-c} - 1$, where $c = 2a - b$. There are $2^a - 2^{a-c}$ fewer bins than desired.

In these cases α and β must be scaled according to the difference between the expected and the true number of bins.

D. Bayesian Bits algorithm

At Figure 5 we provide the algorithm for the forward pass with a Bayesian Bits quantizer.

E. Results on Imagenet

In this section we present more details about the results of our Imagenet experiments on ResNet18. Table 3 provides the accuracy and BOP count for the various methods

we considered, Figure 6 the corresponding plot, whereas Figures 12, 13, 14 and 15 provide the learned ResNet18 architectures using various regularization strengths. It is interesting to see that the learned architectures tend to have higher bit precision for the first and last layers as well as on the weights that correspond to some of the shortcut connections. We also provide the results from the post-training quantization at Tables 4, 5 as well as an updated plot at Figure 7.

Table 3. Results on the Imagenet task with the ResNet18 architecture. We compare against methods from the previous experiments as well as PACT (Choi et al., 2018), (Jacob et al., 2018) and DQ (Uhlich et al., 2020). A * indicates first and last layers in full precision.

Method	# bits W/A	Top-1 Acc. (%)	Rel. GBOPs (%)
Full precision	32/32	69.68	100
(Jacob et al., 2018)	8/8	70.38	6.25
TWN (Li et al., 2017a)	2/32	61.80	5.95
LR-Net (Shayer et al., 2017)*	1/32	59.90	4.58
XNOR-net (Rastegari et al., 2016)	1/1	51.20	0.14
RQ (Louizos et al., 2019)	5/5	65.10	2.54
PACT* (Choi et al., 2018)	4/4	69.20	3.12
PACT* (Choi et al., 2018)	2/2	64.40	2.02
DQ (Uhlich et al., 2020)	Mixed	68.40	2.10
DQ - restricted (Uhlich et al., 2020)	Mixed	68.40	3.09
Bayesian Bits $\mu = 0.03$	Mixed	69.16±0.10	1.93±0.05
Bayesian Bits $\mu = 0.05$	Mixed	67.96±0.22	1.44±0.05
Bayesian Bits $\mu = 0.07$	Mixed	66.27±0.15	1.06±0.02
Bayesian Bits $\mu = 0.2$	Mixed	62.32±0.71	0.68±0.03

Table 4. Results on learning the gates on a small dataset for various regularization strengths. Means and standard errors are computed over 3 training runs for each value of μ .

Regularization	Top-1 Acc. (%)	Rel. GBOPs (%)
$\mu = 0.0001$	69.73 ± 0.06	12.05 ± 0.68
$\mu = 0.0005$	69.69 ± 0.03	7.34 ± 0.34
$\mu = 0.001$	69.63 ± 0.04	6.57 ± 0.14
$\mu = 0.0025$	69.46 ± 0.09	6.14 ± 0.05
$\mu = 0.005$	69.14 ± 0.11	5.45 ± 0.12
$\mu = 0.01$	67.98 ± 0.47	4.55 ± 0.15
$\mu = 0.02$	64.32 ± 0.95	3.74 ± 0.10
$\mu = 0.05$	51.31 ± 1.93	2.90 ± 0.02

Table 5. Results on learning both the gates and scales on a small dataset, for various regularization strengths. Means and standard errors are computed over 3 training runs for each value of μ .

Regularization	Top-1 Acc. (%)	Rel. GBOPs (%)
$\mu = 0.0001$	69.72 ± 0.05	10.87 ± 0.40
$\mu = 0.0005$	69.67 ± 0.03	6.97 ± 0.12
$\mu = 0.001$	69.57 ± 0.02	6.43 ± 0.13
$\mu = 0.0025$	69.47 ± 0.12	5.87 ± 0.21
$\mu = 0.005$	69.28 ± 0.04	4.76 ± 0.06
$\mu = 0.01$	68.31 ± 0.16	3.96 ± 0.00
$\mu = 0.02$	65.44 ± 0.68	2.78 ± 0.15
$\mu = 0.05$	60.20 ± 1.49	1.84 ± 0.06

Algorithm 1 Forward pass with Bayesian bits

Require: Input x, α, β, ϕ
 $\text{clip}(x, \min = \alpha, \max = \beta)$
 $s_2 \leftarrow \frac{\beta - \alpha}{2^2 - 1}, x_2 \leftarrow s_2 \lfloor \frac{x}{s_2} \rfloor$
 $z_2 \leftarrow \text{get_gate}(\phi_2), x_q \leftarrow z_2 x_2$

for b in $\{4, 8, 16, 32\}$ **do**
 $s_b \leftarrow \frac{s_{b/2}}{2^{b/2} + 1}, z_b \leftarrow \text{get_gate}(\phi_b)$
 $\text{.pdfilon}_b \leftarrow s_b \left[\frac{x - (x_2 + \sum_{j < b} \text{.pdfilon}_j)}{s_b} \right]$
 $x_q \leftarrow x_q + z_b \left(\prod_{j < b} z_j \right) \text{.pdfilon}_b$
end for
return x_q

Algorithm 2 Getting the gate during training and inference

Require: Input $\phi, \zeta, \gamma, \beta, t, \text{training}$
if training **then**
 $u \sim U[0, 1], g \leftarrow \log \frac{u}{1-u}, s \leftarrow \sigma((g + \phi)/b)$
 $z \leftarrow \min(1, \max(0, s(\zeta - \gamma) + \gamma))$
else
 $z \leftarrow \mathbb{I} \left[\sigma \left(\beta \log \left(-\frac{\gamma}{\zeta} \right) - \phi \right) < t \right]$
end if
return z

Figure 5. Pseudo-code for the forward pass of the Bayesian Bits quantizer.

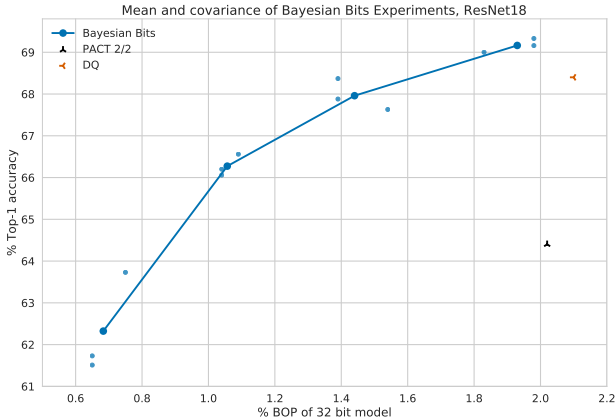


Figure 6. Bayesian Bits Imagenet validation accuracy on ResNet18 for $\mu \in \{0.03, 0.05, 0.07, 0.2\}$. Means and individual runs of 3 training runs for each μ . Note that for the figure in the main text $\mu = 0.2$ had only one run due to time constraints; in this figure $\mu = 0.2$ has three runs as well.

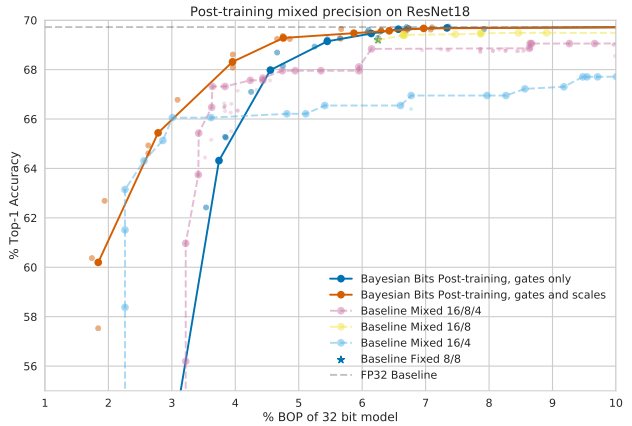


Figure 7. Bayesian Bits Imagenet validation accuracy on ResNet18 for $\mu \in \{0.03, 0.05, 0.07, 0.2\}$. Means and individual runs of 3 training runs for each μ . NB: the corresponding plot in the main text only contains the mean of 2 instead of the reported 3 runs for the leftmost two points in the ‘Bayesian Bits Post-training, gates and scales’ plot. This is fixed in this plot.

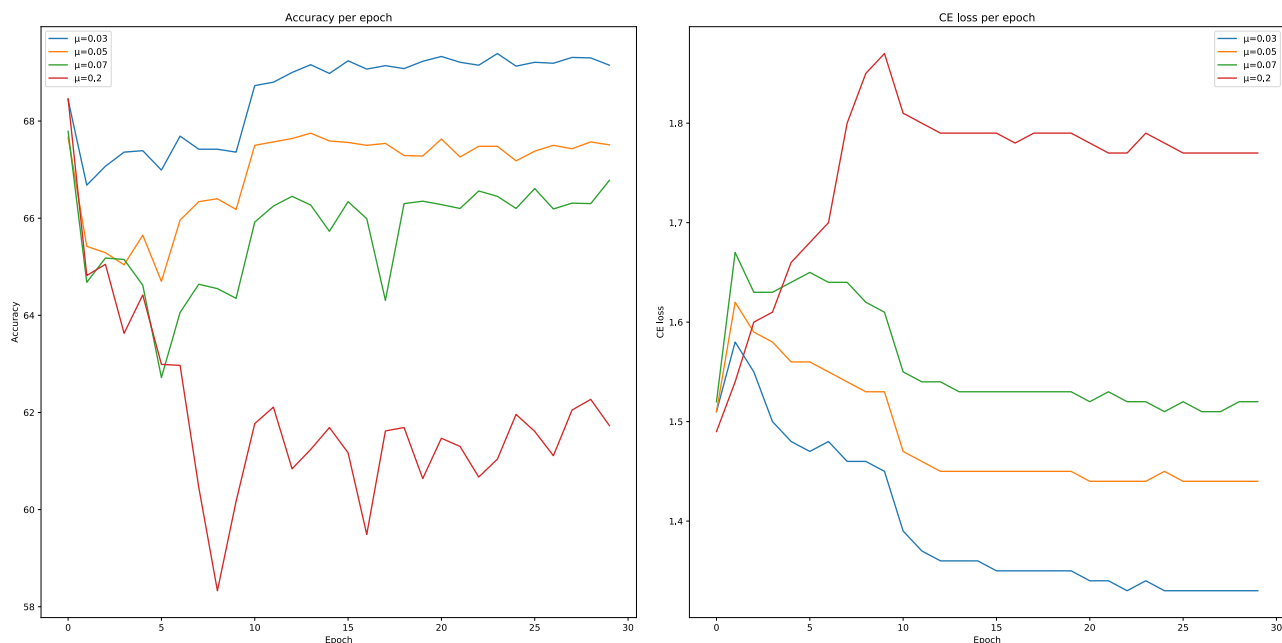


Figure 8. Evolution of validation accuracy and (per epoch average) cross-entropy loss during training of ResNet18 on ImageNet, for $\mu \in \{0.03, 0.05, 0.07, 0.2\}$

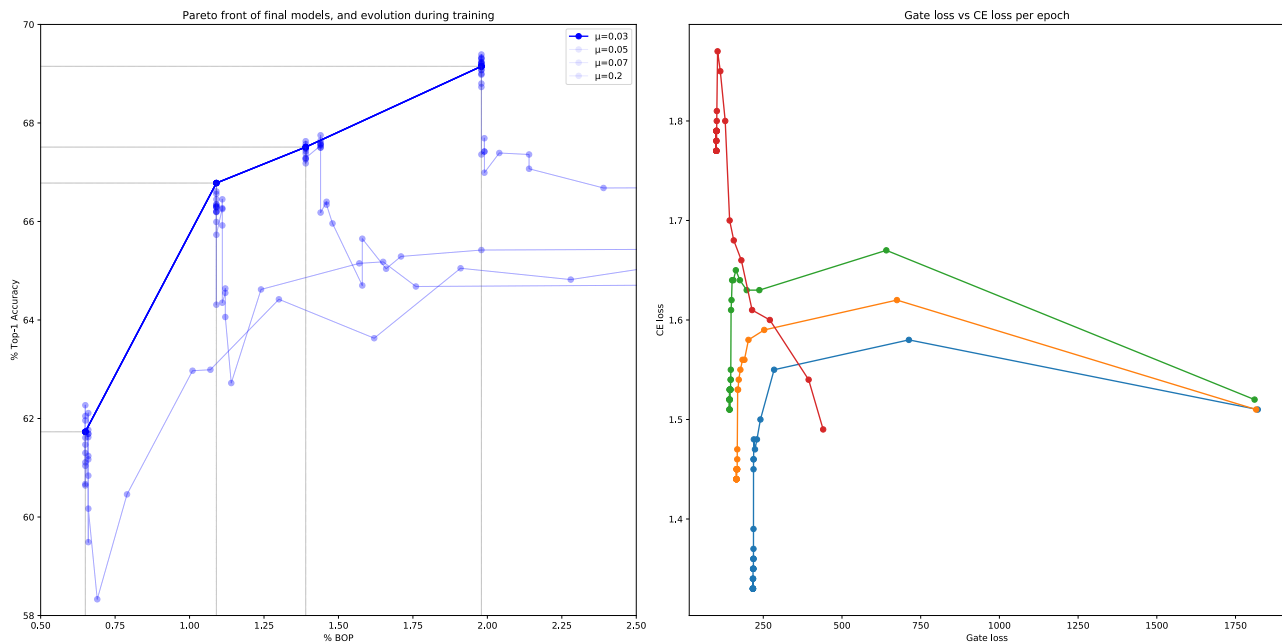


Figure 9. Left plot: Pareto front of final model efficiency vs accuracy trade-offs, including evolution towards final trade-offs. Right plot: Co-evolution of cross-entropy and gate loss per epoch. Both plots show results of training ResNet18 on Imagenet, for $\mu \in \{0.03, 0.05, 0.07, 0.2\}$

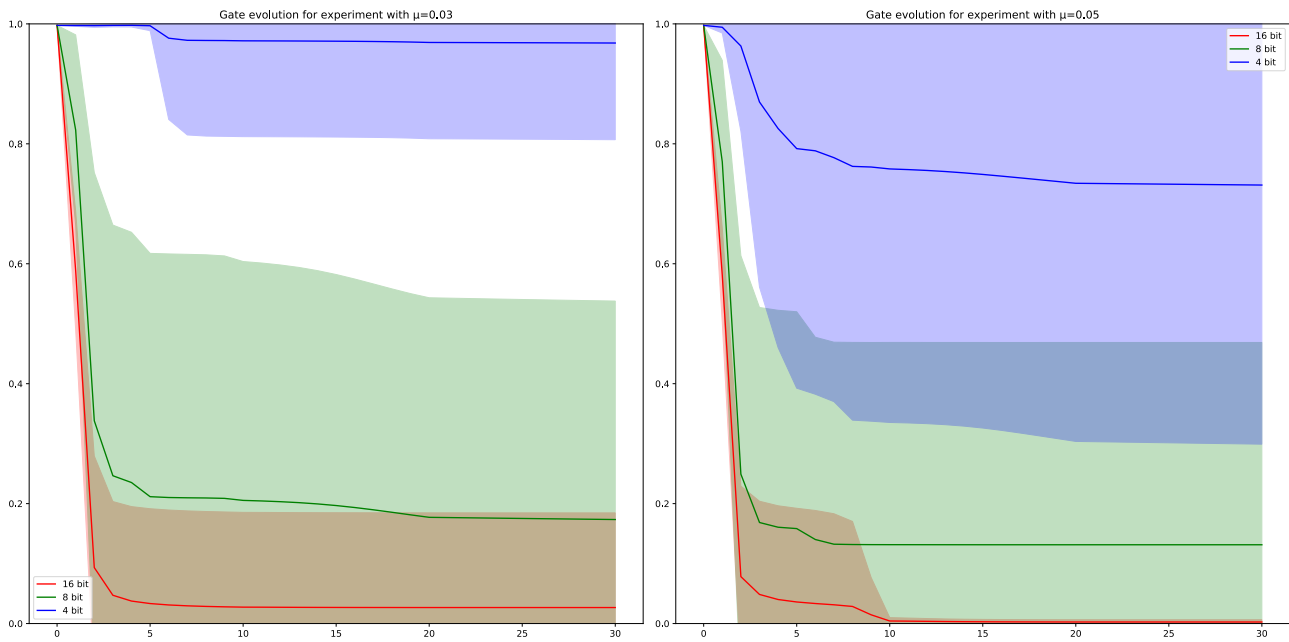


Figure 10. Evolution of training of ResNet18 ImageNet experiments, for $\mu \in \{0.03, 0.05\}$. Mean gate probability with shaded area indicating 1 standard deviation.

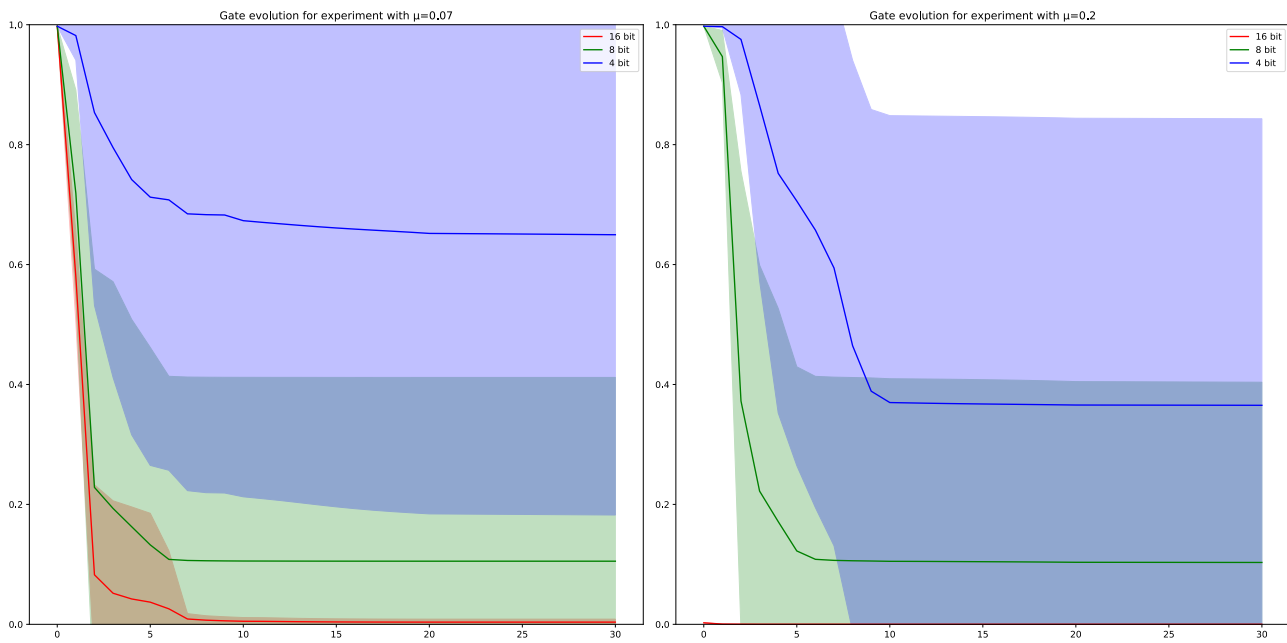


Figure 11. Evolution of training of ResNet18 ImageNet experiments, for $\mu \in \{0.07, 0.2\}$. Mean gate probability with shaded area indicating 1 standard deviation.

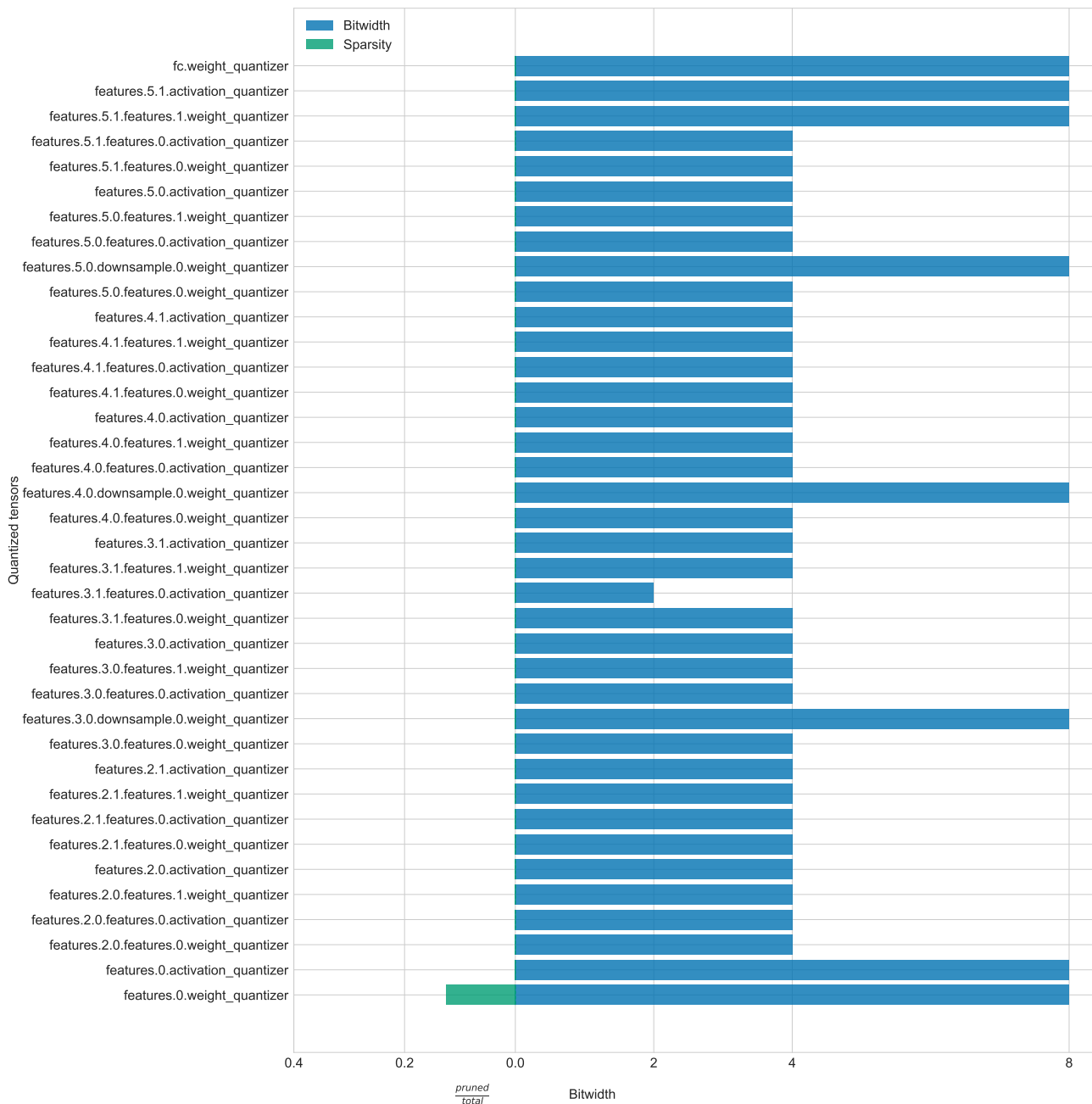


Figure 12. Learned ResNet18 architecture with $\mu = 0.03$.

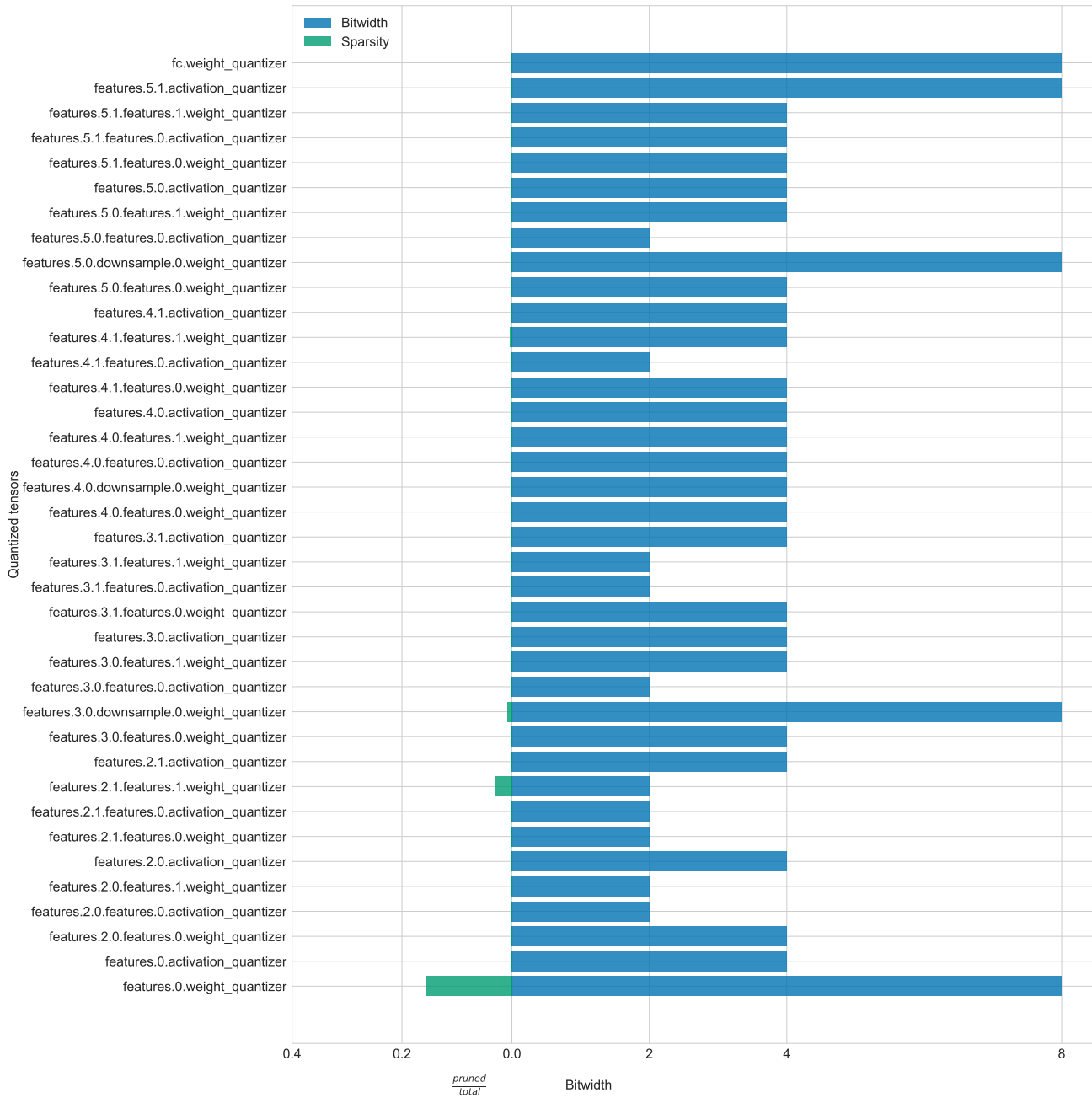


Figure 13. Learned ResNet18 architecture with $\mu = 0.05$.

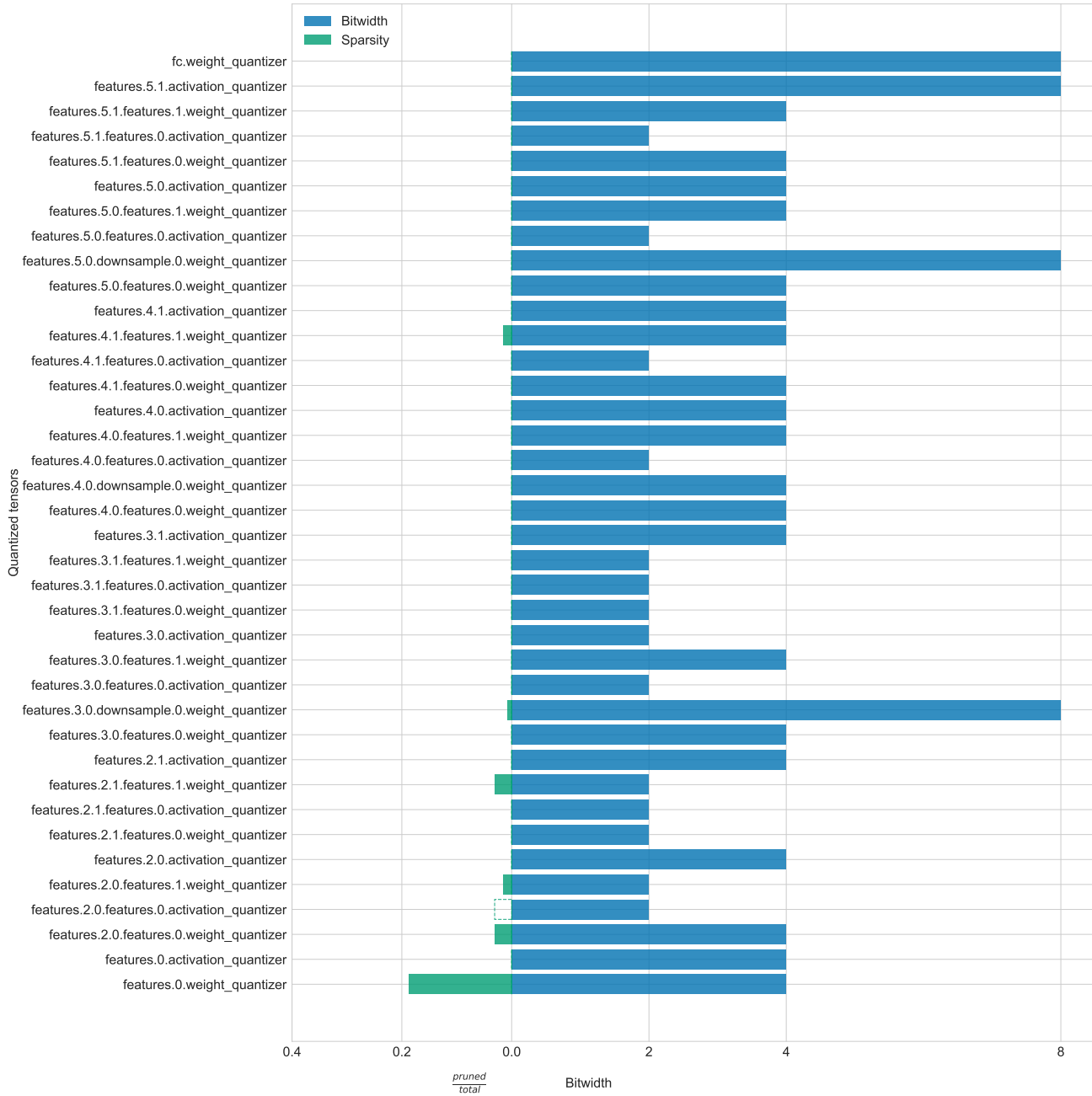


Figure 14. Learned ResNet18 architecture with $\mu = 0.07$.

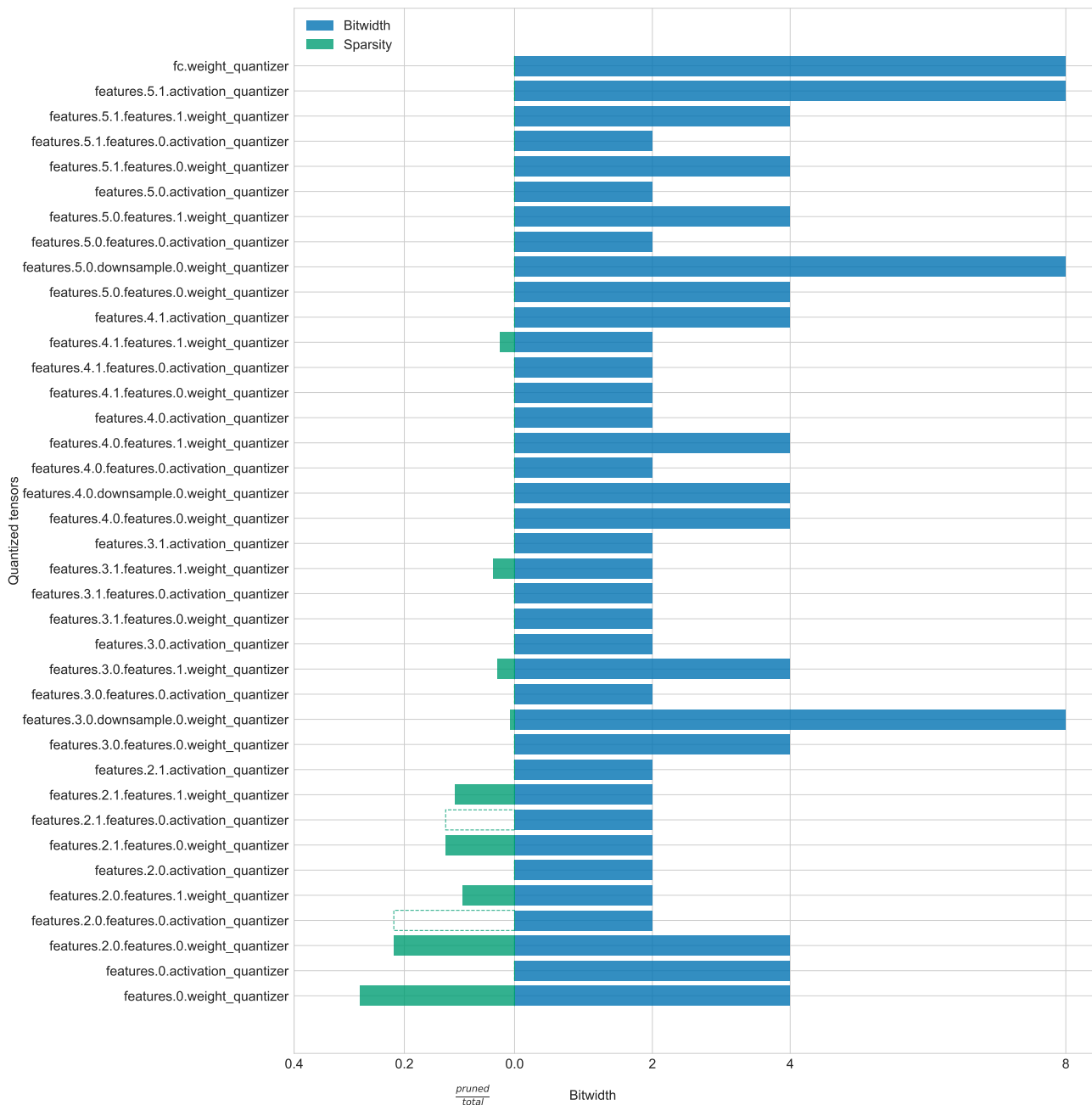


Figure 15. Learned ResNet18 architecture with $\mu = 0.2$.